Chapter 8
Non-invasive Phenotyping Methodologies Enable the Accurate Characterization of Growth and Performance of Shoots and Roots

Marcus Jansen, Francisco Pinto, Kerstin A. Nagel, Dagmar van Dusschoten, Fabio Fiorani, Uwe Rascher, Heike U. Schneider, Achim Walter and Ulrich Schurr

Contents

Abstract Significant improvements of the resource-use efficiency of major crops are required to meet the growing demand of food and feed in the next decades in a sustainable way. Breeding for new varieties and modern crop management aims at obtaining higher and more stable yields by optimizing plant structure and function under different environmental conditions. The development and application of non-invasive methods to estimate plant parameters underlying heritable traits are key enabling components. To address this demand, recently an increasing number of imaging technologies have started to be applied in plant research to analyze various types of genotype collections. Some of these applications are mature and suitable to be scaled-up to higher throughput; others require validation beyond proof-of-concept. In this chapter firstly we present an overview of available methods while stressing the current limitations to be taken into account for correct

M. Jansen (✉) · F. Pinto · K. A. Nagel · D. van Dusschoten · F. Fiorani · U. Rascher · H. U. Schneider · A. Walter · U. Schurr
Institute of Bio- and Geosciences, IBG-2: Plant Sciences, Forschungszentrum, Jülich GmbH, 52425 Jülich, Germany
email: m.jansen@fz-juelich.de

A. Walter
Institute of Agricultural Sciences, ETH Zürich, Universitätstrasse 2, 8092 Zürich, Switzerland

R. Tuberosa et al. (eds.), *Genomics of Plant Genetic Resources,*
DOI 10.1007/978-94-007-7572-5_8,

interpretation of the results. Secondly, we focus on three different case studies by our lab demonstrating the applicability of multispectral, fluorescence, and magnetic resonance imaging for various research questions applicable to controlled environments and to the field. Taken together, these case studies highlight that a variety of non-invasive plant phenotyping methods are essential tools not only for functional genomics, but also for plant selection and breeding. In addition, these experiments underline the need of developing methods tailored to different plant species and at various cultivation systems and scales.

Keywords Plant phenotyping · Non-invasive imaging · Chlorophyll fluorescence · Hyperspectral imaging · Nuclear magnetic resonance imaging (MRI) · Vegetation index

8.1 A Growing Number of Imaging Applications Enrich the Plant Phenotyping Portfolio

Plant phenotypes are dynamic and arise from the complex interaction of genetically encoded molecular networks with multiple environmental factors to which the plant is exposed simultaneously (Walter and Schurr 2005; Walter et al. 2009). In addition, plant responses to the environment are often cumulative and observed phenotypes at a given developmental stage are the result of individual life history. Plant phenotyping however still relies in many cases on traditional methods, e.g. manual measurements or visual estimations (e.g., in the field). To contribute to the selection of genotypes characterized by higher and more stable yields, plant scientists need to tackle this complexity by increased integration of molecular-mechanistic knowledge with accurate measurements of plant performance (Passioura 2010). Also, any technology should be embedded in experimental matrices addressing major factors or their combinations that are relevant for the evaluation of field data (Mittler and Blumwald 2010).

Several imaging methods integrated with appropriate, controlled indoor cultivation systems or by direct deployment of sensors at the field scale offer possible solutions for different research questions applied to shoots and roots (Table 8.1). In this section we first summarize the methodologies that are useful for studying dynamics of whole shoot development and photosynthesis including the evaluation of canopy structure and photosynthesis in the field; secondly we briefly introduce recent advances in root imaging with particular focus on Magnetic Resonance Imaging (MRI).

Automated prototypes using 2D RGB (red-green-blue) or fluorescence imaging have been designed specifically for the extraction of shoot parameters of *Arabidopsis thaliana* (Granier et al. 2006; Walter et al. 2007; Jansen et al. 2009; Arvidsson et al. 2011; Skirycz et al. 2011) or small stature cereals (Berger et al. 2010). These automated systems are suitable for screening genotype panels for variability in (projected) leaf area and developmental dynamics in detailed time course experiments under non-limiting and limiting growth conditions. In addition, shape and geometry of the

Table 8.1 The number of phenotypic parameters that can accurately be measured with imaging techniques is increasing allowing higher throughput both in climate-controlled environments and in the field. We list commonly used and specific imaging methodologies together with recent references (reviews or other significant publications). In addition to the imaging methods, tomographic methods such as Positron Emission Tomography (PET; Jahnke et al. 2009), X-ray Computed Tomography (CT; e.g., Gregory et al. 2003) and neutron tomography (Moradi et al. 2011) are actively being developed for plant roots, and optical scanning methods, such as Laser Induced Fluorescence Transients (LIFT; Kolber et al. 2005), for canopy photosynthesis

Plant parameters	Imaging methods	Experimental setups
Projected shoot area (correlation with biomass); greenness; 2D shoot and root geometry	Color imaging in the visible range (Arvidsson et al. 2011)	Controlled environment
Physiological status of photosystems (PS II)	Chlorophyll fluorescence (Jansen et al. 2009; Rascher et al. 2009)	Controlled environment; field
Canopy temperature	Thermal imaging (Munns et al. 2010)	Controlled environment; field
Various pigment content and canopy properties, such as leaf area index	Imaging spectroscopy/hyperspectral imaging (Ustin and Gamon 2010; Malenovsky et al. 2009)	Field; controlled environment
Structural features in 2D or 3D; water content, diffusion and flow; distribution of specific chemical compounds such as sugars or lipids if highly concentrated	Magnetic Resonance Imaging (MRI) (Simpson et al. 2011; van As 2007; van As et al. 2009)	Controlled environment

shoot is calculated by image analysis as well as photosystems' physiological status. Taken together, these methodologies provide proxies for shoot biomass development (Golzarian et al. 2011) and for the evaluation of responses of the photosynthetic machinery (photosystems and electron transfer) to environmental challenges in controlled or semi-controlled environments (Jansen et al. 2009). However, we consider that applications of fluorescence imaging in controlled environments allowing meaningful interpretation of results are still lacking specifically for non-rosette plants (see also considerations in Berger et al. 2010; Furbank and Tester 2011). Nonetheless, several fluorescence imaging systems are commercially available and, at least for individual leaves, responses to biotic (Osmond et al. 1998) and abiotic triggers (Walter et al. 2004) can be studied in detail. In the field it also became feasible recently to detect sun-induced fluorescence using the Fraunhofer Line Depth (FLD) detection principle (Moya et al. 2004; Rascher et al. 2009).

In addition to visible and fluorescence imaging, thermal imaging is increasingly used to map canopy temperature and for establishing screening protocols to identify in particular genotypes with high water use efficiency (Munns et al. 2010). Although thermography is an attractive technique, we stress that result interpretation and its use as a proxy for transpiration requires careful experimental calibration and a deep understanding of the physical principles of heat exchange at the leaf surface (Kümmerlen et al. 1999).

Recently, spectral analysis approaches have arisen as a versatile and accessible tool for non-destructive observation of vegetation, and sensors detecting spectral distribution of the radiation reflected by vegetation are becoming affordable and more widely used. The radiative properties of plant leaves or canopies can be used for determining structure and physiological status of the vegetation. The portion of radiation that is reflected, absorbed and transmitted for a specific wavelength at the leaf or canopy scale is determined by: (i) leaf structure and chemical composition; (ii) optical properties of the canopy and soil; and (iii) external effects like illumination and the observation geometry, which is defined by the position of the sun, vegetation and the sensor (Goel 1988, 1989; Chen et al. 2000). Optical spectroscopy uses mainly the reflected part of the radiation to retrieve information about biochemical and structural properties of vegetation. For instance, the spectral reflectance of vegetation is characterized by a low reflectivity in the visible part of the spectrum (400–700 nm) due to a strong absorption by photosynthetic pigments, while a high reflectivity in the near infrared (700–1100 nm) is produced by a high scattering of light by the leaf mesophyll tissues (Knipling 1970; Rascher et al. 2010). In addition, in the shortwave infrared part of the spectrum (1100–2500 nm) the reflectance intensity is affected by the water content of plant tissues (Danson et al. 1992, Rollin and Milton, 1998, Rascher et al. 2010).

The characteristics of optical spectroscopy make this technique highly suitable for fast, non-invasive and reproducible measurements on plant function. The addition of spatial information by imaging spectroscopy offers new opportunities for plant phenotyping. The data can be seen as a cube, with the X and Y axes corresponding to two spatial dimensions and the Z axes to the spectrum (Fig. 8.1). For each pixel, a continuous spectrum of reflectance is obtained. The interpretation of the data is not always simple as the spectral reflectance is strongly affected by the spatial distribution of the different elements involved in the interaction between radiation and vegetation (Goel 1988; Myneni et al. 1989; Barton and North 2001).

Research on the dynamics of root growth requires different methodological approaches compared to research on shoots. This field of research experienced substantial improvements in recent years because of a series of technological developments. Rhizotron cultivation with protocols using artificial substrates such as agar and soil mixtures, as well as natural soils, was combined with different techniques visualizing root systems, such as cameras (Armengaud et al. 2009; Hargreaves et al. 2009; Nagel et al. 2009, 2012; Rascher et al. 2011) or neutron radiography (Carminati et al. 2010). Combination with appropriate analytical tools yields 2D data sets of root systems suitable for calculating features of root system architecture such as root diameter, root length, density, and branching angles (Hagreaves et al. 2009; Nagel et al. 2009, 2012; Rascher et al. 2011). For visualization of roots in three-dimensional container systems protocols have been developed for plant cultivation in transparent gellan gum for image acquisition with cameras (Iyer-Pascuzzi et al. 2010; Clark et al. 2011). For opaque systems, i.e. roots in soil, substantial efforts have been made to implement suitable measuring protocols with X-ray computed tomography (CT; Heeraman et al. 1997; Gregory et al. 2003; Pierret et al. 2003; Hargreaves et al. 2009), neutron tomography (Moradi et al. 2011) and nuclear magnetic

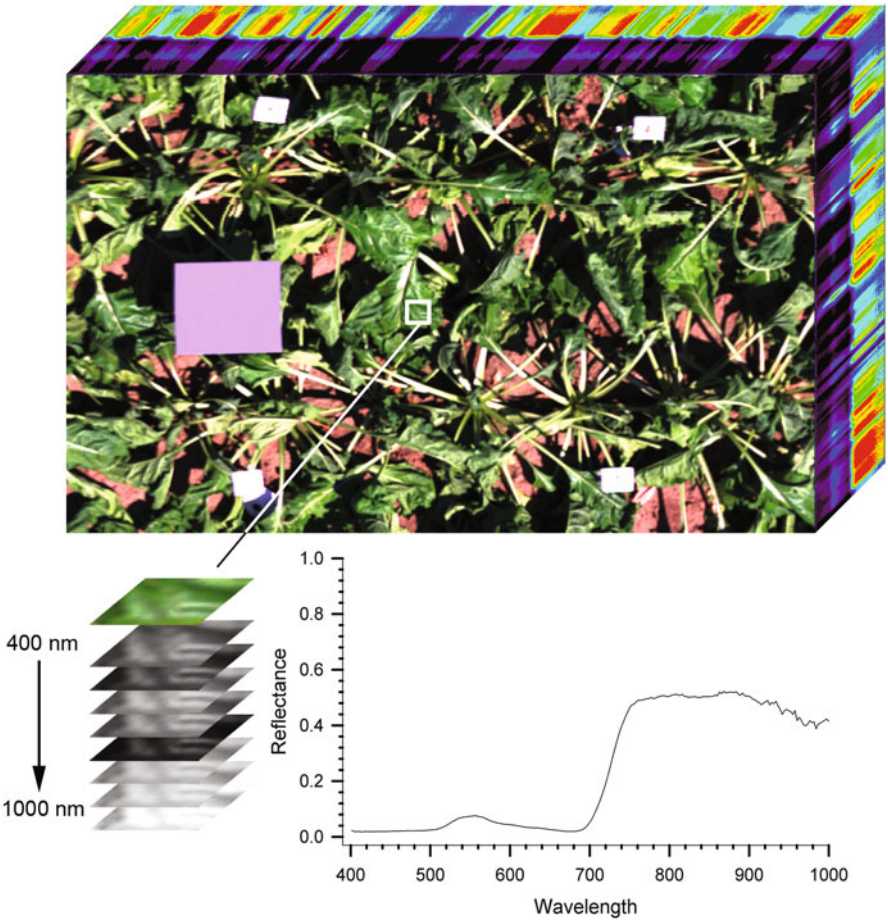

Fig. 8.1 Scheme of 3-dimensional data cube from a sugar beet canopy obtained by imaging spectroscopy. The hyperspectral data cube was taken from four meters above the canopy in the experimental field site Klein-Altendorf of the University of Bonn, Germany. Two dimensions account for the spatial information, while the third dimension codes for the spectral information. Each pixel in a scene is associated with a continuous spectrum of relative reflectance. In the left part of the image, the gray reflectance standard is visible. The stack (*lower left corner*) exemplifies the intensity of some spectral bands between 400 and 1000 nm, taken from the region of interest. The reflectance spectrum (*lower right side*) gives the hyperspectral reflectance values (relative to incoming radiation) of this region of interest

resonance imaging (MRI; e.g. Bottomley et al. 1986, 1993; Brown et al. 1991; Menzel et al. 2007; Jahnke et al. 2009; Nagel et al. 2009; Rascher et al. 2011). A recent summary of achievements in research on root system architecture using CT is given by Zhu et al. (2011). Here we will focus on describing the potential of MRI for root phenotyping.

In brief, MRI detects signals from protons (hydrogen nuclei) in a given specimen. The signals are measured in a spatial array and plotted as an image, where the brightness of the pixels is roughly proportional to the proton density. Though being

particularly valuable for investigations on plant organs in opaque media such as soil, application of MRI for studies of entire root systems in soil is still very scarce and challenging and, thus, far from being a routine approach for phenotyping. However, when ferromagnetic particles are removed and proper soil types and soil moisture are chosen, decent MRI images can be acquired (e.g. Rogers and Bottomley 1987; Brown et al. 1991; Menzel et al. 2007; Hillnhütter et al. 2012; Rascher et al. 2011). A very good case study of Brown et al. (1991) showed that MRI with special soil mixtures can even allow for accurate non-invasive quantification of root length during growth. So far, most MRI studies on root systems did not focus much on measuring speed. Rather, to achieve high-quality images they used comparably long measuring times per data set ranging from tens of minutes up to hours (Brown et al. 1991; Hillnhütter et al. 2012). However, development of fast measuring and data evaluation protocols as shown for other MRI applications (e.g. Meininger et al. 1997; Rokitta et al. 1999), in combination with automation of sample handling, would allow for the use of MRI for moderate-throughput scanning of root systems for phenotyping purposes, similar to its employment in food and materials sciences.

Each phenotyping method opens a specific window to an aspect of the multitude of phenotypic properties that make up structure and functionality of a whole plant. In the following sections we present three different case studies that highlight the range of different imaging applications (spectroscopic and fluorescence imaging and MRI) in both controlled environment and field experiments and for different plant species (*Arabidopsis*, barley, petunia and poplar). Taken together, these examples show that selected technologies can be used to address relevant biological questions concerning variability of plant responses to the environment (case studies 1–3) and also be used for advanced pre-selection protocols of valuable breeding populations (case study 3).

8.2 Precision Phenotyping of Canopies Structure and Photosynthetic Performance

In optical spectroscopy of vegetation, numerous analytical procedures exist for the extraction of information from, and interpretation of, reflectance signatures based on the analysis of either continuous spectra or selected spectral regions or wavelengths. The analysis of continuous spectra may be the most complete way but, due to the high number of parameters that can affect spectral features, normally is not a straightforward process. In fact, each wavelength could be considered as a variable. To simplify the analysis, scientists have focused on particular wavelengths that are directly related to reflectance properties of specific molecules or that could represent a proxy to identify stress response at the leaf or canopy level. The combination of reflectance values at two or more specific spectral bands yields so-called vegetation indices (VIs) (Jackson and Huete 1991). In the past decades, a great number of VIs has been developed to quantify (i) pigment contents, (ii) functional and physiological properties, and (iii) structural properties of plants and canopies. VIs offer the following advantages: (i) a small amount of spectral bands is required, simplifying the

Table 8.2 List of the most used vegetation indices. In the formulas R_x denote for relative reflectance at the wavelength or spectral region that is specified in the subscript, i.e. R_{red} codes for the relative reflectance in the red light spectrum and R_{670} codes for reflectance at 670 nm

Vegetation index	Formula
Normalized difference vegetation index	$NDVI = \frac{R_{NIR}-R_{red}}{R_{NIR}+R_{red}}$
Simple ratio	$SR = \frac{R_{NIR}}{R_{red}}$
Enhanced vegetation index	$EVI = 2.5\frac{R_{NIR}-R_{RED}}{R_{NIR}+6\times R_{RED}-7.5\times R_{BLUE}+1}$
Carotenoids reflectance index 1	$CRI1 = \frac{1}{R_{510}} - \frac{1}{R_{550}}$
Carotenoids reflectance index 2	$CRI2 = \frac{1}{R_{510}} - \frac{1}{R_{700}}$
Anthocyanin reflectance index 1	$ARI1 = \frac{1}{R_{550}} - \frac{1}{R_{700}}$
Anthocyanin reflectance index 2	$ARI2 = R_{800} \times \left[\frac{1}{R_{550}} - \frac{1}{R_{700}}\right]$
Plant senescence reflectance index	$PSRI = \frac{R_{680}-R_{500}}{R_{750}}$
Photochemical reflectance index	$PRI = \frac{R_{531}-R_{570}}{R_{531}-R_{570}}$

equipment needed for the measurements; (ii) simple calculation; and (iii) reduced use of computing resources. However, by using VIs major portions of the continuous spectrum are not considered and the capability of modern spectrometers is not fully exploited. Thus, VIs are a simple way to quantify plant traits, but may not be sufficient to quantify complex processes that are related to subtle changes within the absorption properties of leaves and canopies, such as the functional reorganization of pigments associated with photosynthetic light protection. Additionally, VIs are known to be greatly affected by the observation geometry and vegetation architecture and may be dependent on the spatial scale of observations and orientation between the plant and the sensor (Blackburn 2007).

Despite the constraints that VIs present, this method is becoming widely adopted among researchers in the area of breeding, precision agriculture and remote sensing, mainly due to its simplicity. Moreover, the introduction of imaging spectroscopy offers a simple way for estimation of functional and structural traits through spatially resolved VIs at leaf and canopy level. A study case is presented in the following, where VIs estimated from hyperspectral images were taken over crop canopies of four barley varieties (Barke, Mauritia, Sebastian, and Wiebke) grown using the standard agricultural management of barley under rainfed conditions.

Measurements were taken at five different dates during the vegetation period, around solar noon ($\pm$ 2 h). An imaging spectrometer PS V10E (Spectral Imaging Ltd., Finland) was used to obtain the spectrum of vegetation in the visible/ near infrared part of the spectrum (350–1050 nm). Images were acquired at 4 m height in nadir position, each of them covering ground area of 1 $\times$ 1.5 m within each experimental plot. A white panel with Lambertian reflectance was located in each scene and then used as a reference of solar radiation for the reflectance estimation of each pixel within the image.

Table 8.2 shows a selection of VIs that are potentially useful for phenotyping of plant canopies. Traits like Leaf Area Index (LAI), pigment content or even

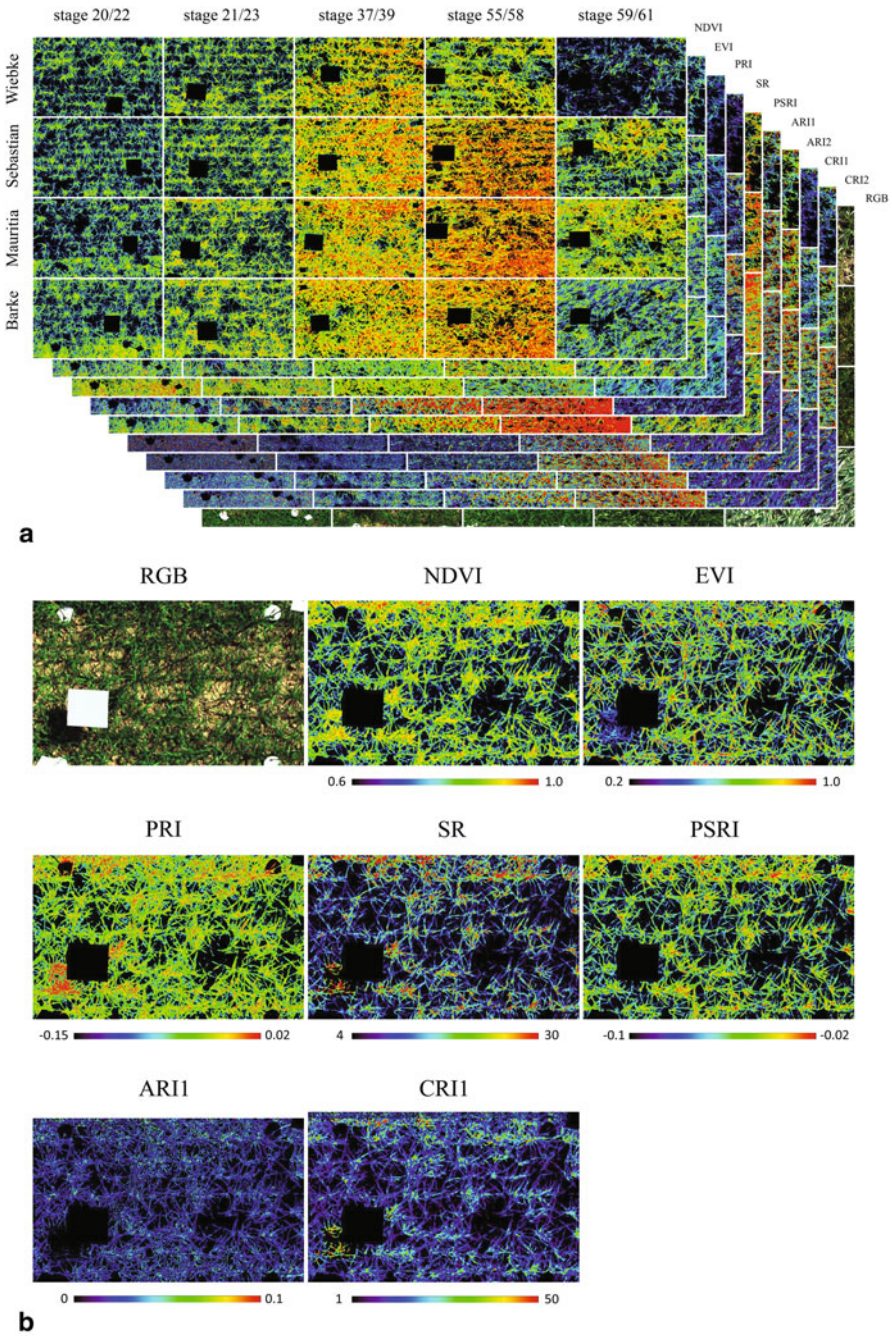

Fig. 8.2 Imaging spectroscopy and the seasonal changes of relevant vegetation indices (VIs) in a barley canopy. VIs were calculated from hyperspectral images in four varieties of barley at five different growth stages according to Zadoks scale (Zadoks et al, 1974) recorded 4 m above the

photosynthetic efficiency have shown correlations with some of these VIs. In this study case, changes in values and spatial distribution through the vegetation period can be observed for most of the VIs (Fig. 8.2a, rows). Additionally, it is also possible to observe some differences between the varieties compared at the same date (Fig. 8.2a, columns). Spatial variations within one image are related to both, differences in plant function and differences in illumination conditions determined by the canopy structure.

It has been observed that increases of grain productivity in crops are more related to higher values of vegetative biomass and increases of photosynthesis per unit land area than to higher rates of leaf photosynthesis itself (Richards 2000). In this context, estimation of LAI and biomass are of particular interest to evaluate whether the canopy structure presents optimal conditions for light capture and biomass production. These two parameters have shown good correlation with those VIs based on the differences in reflectance between the red region (RED) and the near infrared (NIR), which is a characteristic feature of green plant tissues (Christensen and Goudriaan 1993; Turner et al. 1999). Two of these indices which are most frequently used are the Normalized Difference Vegetation Index (NDVI) and the Simple Ratio (SR, Table 8.2).

NDVI can be used to track seasonal changes in barley canopies that can be related with structural changes of the canopy or plant cover (Fig. 8.2). For the same reason, it has also been used for indirect estimation of absorbed photosynthetically active radiation (APAR) (Christensen and Goudriaan 1993; Hansen and Schjoerring 2003; Turner et al. 1999).

When observing differences of NDVI within one image (Fig. 8.2b) it can be noticed that in zones with higher density of plants, like in the borders of the images or in the leaves of the upper layer (center of the plant looking from above), values are higher. From the pictures in Fig. 8.2 it becomes obvious that only leaves of the outer, visible canopy contribute to the NDVI image and there is no superimposed information from lower canopy layers.

There is evidence that NDVI correlates with leaf chlorophyll content (Haboudane et al. 2004), meaning that this index can be potentially used to establish phenological changes based in this pigment or observed nitrogen deficit (Hansen and Schjoerring 2003). In our images, seasonal changes observed in NDVI values (Fig. 8.2a, rows) may be closely related with the seasonal changes in chlorophyll content. It can be observed, for example, that at earlier stages, the values of NDVI are more homogeneous and lower than values at the middle of the growing season (Fig. 8.2a). What is more, a dramatic reduction of NDVI is observed towards the last measuring date, indicating a reduction of green material, which coincided with the ripening of the ears and an increased amount of yellow leaves.

Simple Ratio (SR) and Enhanced Vegetation Index (EVI, Table 8.2) were developed in remote sensing science and were shown to give a better estimation at

Fig. 8.2 canopy. White elements are reference targets that are used for calibration. **a** Seasonal variations of NDVI values measured on five growth stages during the vegetation cycle and in comparison of four varieties. **b** Different VIs calculated over a canopy of barley var. Mauritia at growth stage 21/23 (Zadoks scale)

LAI values of dense vegetation. The EVI adds additionally the reflectance value in the blue region to correct the signal from soil background and reduces atmospheric influences including aerosol scattering. However, remote-sensing science normally works with very coarse spatial resolution and single pixels are spectral aggregates over several meters or even kilometers. Consequently, a large number of objects are spectrally mixed in the spectrum for each pixel. Using these VIs in plant and canopy imaging has several disadvantages. EVI, for example, is greatly affected by shadows; significantly lower values appear in shaded areas in comparison to sun illuminated ones (see shadow in lower left corner of EVI image in Fig. 8.2). SR also is affected by shadows (Fig. 8.2), but may provide the advantage to contain also information related to occluded leaf patches in dense canopies (Fig. 8.2b with dense canopy).

Seasonal changes were also observed in VIs, which can be used to estimate other pigments of the leaves (seasonal image data in lower stacks of Fig. 8.2). That is the case of the Carotenoids Reflectance Index 1 and 2 (CRI1 and CRI2, Table 8.2) and the Anthocyanin Reflectance Index 1 and 2 (ARI1 and ARI2, Table 8.2). These indices are based on the strong absorption that these pigments have at 510 nm (carotenoids) and at 550 nm (anthocyanin). Therefore, variations of reflectance values at these specific wavelengths are directly related with the variation in concentrations of these pigments at leaf level. However, chlorophyll also affects the reflectance in this part of the spectrum and therefore is in part eliminated by subtracting reflectance values at wavelengths where chlorophyll just absorbs (700 nm).

Besides chlorophyll, carotenoids are the main pigments of the leaves. Specific structural and physiological functions have been attributed to them such as: energy transfer, participation of light harvest, antioxidants, structural role in photosynthetic membranes, and quenching of chlorophyll excited states (Gitelson et al. 2002). These pigments are located mainly in the vacuoles of epidermal cells and there is evidence that they play an important role in photoprotection by filtering part of the UV radiation and excessive Photosynthetic Active Radiation (PAR). Therefore their biosynthesis may be induced by stresses that lead to a reduction of photosynthetic efficiency, like for example deficiencies in nitrogen, high UV radiation or pathogen infections (Gitelson et al. 2009).

However, only a small number of studies have investigated these indices and their implications at the canopy scale (Blackburn 2007). It must be taken into account that these indices use very specific wavelengths that can be easily confounded by different factors while measuring at this level. Changes in the observation geometry or the presence of shadows can lead to wrong estimations of anthocyanins and carotenoids (Verrelst et al. 2008). A good example can be seen in Fig. 8.2b, where the shadow produced in the lower left corner leads to an underestimation of anthocyanin and an overestimation of carotenoids.

Seasonal changes of these indices, as well as changes of chlorophyll estimated using NDVI, must be interpreted with care. Leaf senescence for example is characterized by a strong reduction of the ratio between chlorophylls and carotenoids. However, in our images, NDVI shows a similar time course as CRI indices. The reason may be structural factors that are increasing values of NDVI or producing an overestimation of the carotenoids indices. Alternatively, the reflectance at

the specific wavelengths used in CRI, as well as for ARI, may have been strongly affected by high content of chlorophyll. Merzlyak et al. (1997) suggest that indices like CRI1 and CRI2 are not suitable for observing leaf senescence because they have shown to be less sensitive at low concentrations of pigments. The Plant Senescence Reflectance Index (PSRI, Table 8.2) was designed to maximize the sensitivity to the ratio of carotenoids to chlorophyll (Merzlyak et al. 1999). As a consequence, an increase in PSRI indicates a decrease of chlorophyll content and the onset of canopy senescence. In this context, the behavior of PSRI is in agreement with the changes observed in CRI1 and CRI2. However, it is still unclear to which magnitude this index can be affected by structural or illumination factors.

Although traits such as LAI and pigment content can work as indirect estimators of the physiological status of the crop, they usually fail when trying to estimate the actual photosynthetic efficiency of the vegetation. So far, the best methodologies for measuring photosynthesis are based on measurements at leaf level, and have succeeded very seldom in up scaling them to canopy or crop. The Photochemical Reflectance Index (PRI), for instance, is a vegetation index designed to detect changes in the xanthophyll pool composition associated with reduction of light use efficiency (Gamon et al. 1990, 1992; Rascher et al. 2007). A decrease in photochemical efficiency via violaxanthin de-epoxidation due to excess of radiation leads to an increase of the absorption at 531 nm, and therefore to lower values of PRI (Table 8.2). It is worthy to note, however, that there is some confusion in the literature since in some studies the formula is inverted and thus depending on specific definition, the PRI may be positively or negatively correlated with photosynthetic efficiency.

In Fig. 8.2, low values of PRI coincide with the part of vegetation which is under the higher light conditions. In contrast, it can be observed that in general higher values of PRI occur where vegetation is in the shadow. Higher values of PRI are also found in the upper part of the canopy. In this case, the vertical orientation of the leaves in these regions has a strong effect on the PRI values, indicating that canopy structure is an important point to consider for a proper interpretation of this index. It has been well established that PRI is strongly affected by the plant/canopy structure and the geometry of the observation (Barton and North 2001; Verrelst et al. 2008), showing large variability even among plants with the same photosynthetic capacity (Guo and Trotter 2004).

PRI decreased strongly in barley canopies at day 188 (growth stage 59-60 according to Zadok scale) of our measurement series, which coincided with a strong increase of anthocyanin, carotenoids and senescence indices, but also with high values of NDVI. This could mean that lower values of PRI at this date indicate a lower photosynthetic efficiency driven by the loss of chlorophyll that can be deduced from the high values of ARI, CRI and PSRI. Alternatively, high NDVI values at this stage of crop development may be explained by a high LAI and biomass. Differences in PRI have been reported to be affected by changes in leaf pigment level (chlorophyll), which would be a reason why PRI is correlated to seasonal changes in light use efficiency (LUE) (Stylinski et al. 2002).

PRI has been studied in numerous analyses using different classes of vegetation from leaf to ecosystem level, at different time scales. Garbulsky et al. (2011) performed a meta-analysis based on more than 80 publications about PRI, and concluded that in general, this index shows a good correlation with different physiological variables at different time and spatial scales, especially with effective quantum yield (ΔF/Fm') and LUE. At the canopy level, the good estimation of LUE by PRI suggests that optical properties of the upper canopy region can be used to estimate the photosynthetic efficiency of the whole canopy (Garbulsky et al. 2011).

As shown above, drawing conclusions derived from VIs is often complex. A main issue at canopy scale is its complex 3D structure, in which the reflected radiation is highly determined not only by the external light conditions but also by its architecture. In this regard, imaging spectroscopy on the canopy scale offers the unique advantage to have the spatial information that allows identifying specific elements within the canopy or specific regions under different light conditions. Moreover, its combination with methods for 3D canopy reconstruction can be a powerful tool for a better understanding of the light-canopy-sensor interaction (Rascher et al. 2011) and provide information how spectral reflectance and VIs are affected by the canopy structure.

Although VIs are an easy and fast way to obtain information on some traits in vegetation, they can greatly be influenced by other factors and thus their robustness is limited. Thus, quantitative conclusions have to be drawn with care. It is likely that vegetation properties or physiological changes rather affect larger regions of the spectrum than narrow bands. Analyses of continuous spectra are promising, but imply the use of complex statistics and modeling. Some of the current and most powerful methodologies are Partial Least Square Regression (PLSR; Feilhauer et al. 2010), supervised and un-supervised endmember selection and unmixing, continuous support vector machines (Hostert et al. 2005), multi-block analysis (Eiden et al. 2007) or simplex volume maximization (Römer et al. 2012). All these methods were shown to provide significantly more accurate results than the use of VIs; however, their application for phenotyping purposes requires major adaptation of computer algorithms and data processing. We nevertheless expect that such advanced methods may become more widely used in the future. However, to date, they remain restricted to a few case studies.

8.3 Non-invasive Fluorescence Imaging of Arabidopsis Enables the Quantification of Phenotypic Diversity Driven by Genetic and Environmental Factors

Besides the selection of appropriate measurement sensors and indicators, minimizing unintended environmental influences on phenotypes by standardization of procedures and randomization of plant layouts is crucial to diminish the influence of external factors on the experimental outcome (Hurlbert 1984; Schilling et al. 2008). By

developing and implementing such standard operation protocols (SOP) of Good Phenotyping Practice (GPP), phenotypic variability can be assigned to different genetic properties of ecotypes, or to environmental factors that were tested, respectively. Such genetic and phenotypic diversity of *A. thaliana* can be exemplified by comparing phenotypes of plants grown in different environments and of ecotypes originating from various geographical locations.

In the case study presented here we set out to validate our *Arabidopsis* screening platform, GROWSCREEN FLUORO (Jansen et al. 2009) to establish detailed SOPs including the management of growth conditions and analyze the sensitivity of commonly used ecotypes to variable levels of irradiance, water supply, and nutrients. *A. thaliana* plants were grown in a growth chamber at controlled non-limiting environmental conditions while ecotypes and other environmental conditions were varied systematically.

Growth as well as shoot architecture responded strongly when one specific ecotype (Col-0) was exposed to different water and light regimes (experiment 1; Fig. 8.3a–d) or different types of soil substrates (experiment 2; Fig. 8.3e). These responses indicate the strong dependency of the measured traits on environmental conditions. In order to assess phenotypic responses to genomic differences, we grew nine different ecotypes, Be-0, C24, Col-0, Cvi, Eri-1, Hog, Ler, Sha, and Ws-2 in a climate chamber in one set of environmental conditions (experiment 3; Fig. 8.3f). Ecotypes displayed strong differences in size and shape of single leaves and rosettes.

As part of the SOP all plants were treated identically before the analysis and before exposing them to varied environmental conditions to maximize differences in phenotypes: all plants were pre-germinated in soil-filled trays. After cotyledon unfolding, they were transferred to single-plant pots filled with equal volumes of substrate according to Table 8.3 and were watered up to maximum water holding capacity. Thereafter water was withheld until reaching the targeted water holding capacity (Table 8.3) and then the target value was maintained by controlled irrigation. Shoot parameters such as projected leaf area, rosette morphology, and chlorophyll fluorescence were quantified using the screening system GROWSCREEN FLUORO (Jansen et al. 2009).

In experiments 1 and 2, one ecotype, Col-0, was chosen to test its sensitivity to crucial environmental conditions. Typical factors which are varied in laboratory experiments are e.g. growth media, watering intensity and frequency, and light intensity and quality (PAR). Some of these factors were systematically varied to assess their impact (see Table 8.3). With exception of the nearly nutrient-free peat soil (low-N soil), all variable factors were chosen to be in a range that does not create extreme conditions and is congruent to what is described for unstressed growth of *A. thaliana* in many published studies (e.g. Weigel and Glazebrook 2002 or http://www.hort.purdue.edu/hort/facilities/greenhouse/101exp.shtml).

Whereas the choice of substrate is a single event at the beginning of the cultivation period, light and water supply are subject to fluctuations or intended changes in experiments in growth chamber or glasshouses during experimental protocols. To assess effects of differences in light and irrigation regimes, Col-0 plants were

Fig. 8.3 *A. thaliana* shoot phenotypes. Sample images were taken at the end of the vegetative growth period in each set. Phenotypic variability of ecotype Col-0 caused by cultivation conditions (a–d, experiment 1): moderate light, moist soil (**a**), low light, moist soil (**b**), moderate light, wet soil (**c**), and low light, wet soil (**d**), or by different growth media (**e**, experiment 2), or phenotypic variability of different ecotypes (**f**, experiment 3); scale bar = 10 cm

Table 8.3 Phenotypic diversity of *A. thaliana* driven by genetic and environmental factors was exemplary shown by analyzing the ecotype Col-0 under different environmental scenarios (experiment 1: different water and light regimes and experiment 2: different growth media and by comparing ecotypes originating from various geographical locations (experiment 3). All plants were grown under 22°C day and 18°C night temperature, 60 % relative air humidity, and an 8 h/16 h day-night-regime

Exp.	Ecotypes	Soil	Water supply	Light
1	Col-0	Mixed soil: Peat-sand-pumice mixture (NPK 12-12-17)	Moist: 60 % or wet: 95 % of max. water holding capacity	80, 140, or 200 μmol m^{-2} s^{-1}
2	Col-0	Mixed soil (NPK 12-12-17), high-N soil (peat, NPK 25-30-40), intermediate-N soil (peat, NPK 12-14-24) or low-N soil (peat, NPK 5-8-8)	Moist: 60 % of max. water holding capacity	200 μmol m^{-2} s^{-1}
3	Be-0, C24, Col-0, Cvi, Eri-1, Hog, Ler, Sha, Ws-2	Mixed soil (NPK 12-12-17)	Moist: 60 % of max. water-holding capacity	200 μmol m^{-2} s^{-1}

subjected to different light and irrigation regimes (experiment 1). Plants provided with the largest amount of water and highest intensity of light reached the largest final projected leaf area (A_{PT}) of approximately 45 cm^2 (Fig. 8.4a). In contrast, plants with the lowest supply of water and light reached an A_{PT} of 7 cm^2 only. Reduction of only one of the two environmental factors, light or water, resulted in plants with similar final leaf area size (18 cm^2; Fig. 8.4a). However, the plants reached the final leaf area with pronounced differences in growth rates. At higher light conditions (200 μmol m^{-2} s^{-1}) but reduced water availability (moist soil) plants exhibited initially high growth rates, but leaf expansion rate decreased later, whereas the growth rates of plants grown at low light (80 μmol m^{-2} s^{-1}) and high soil moisture (wet soil) conditions were low at the onset of the experiment and increased at later stages. Besides differences in growth rates, plants were morphologically distinct: plants grown at 200 μmol m^{-2} s^{-1} in moist soil had shorter petioles—indicated by higher rosette compactness—than all other plant populations (Fig. 8.4b). Plants grown at the same light regime in wet soil treatment increased rosette compactness from 35 d a.s. onwards due to younger leaves growing into spaces between the long-petiole older leaves. With respect to chlorophyll fluorescence all sets of plants had an initial period with variable F_v/F_m. Later on, the efficiency of PSII in plants grown at 200 μmol m^{-2} s^{-1} stabilized at 0.75, while it stabilized at 0.73 in plants grown at lower light intensities (Fig. 8.4c). The different water availability had minor impact on F_v/F_m.

As could be shown, the difference in irrigation of only 10 % (w/w) more water between wet and moist soil treatment and in light intensity of 120 μmol m^{-2} s^{-1} was sufficient to result in pronounced variations in A_{PT} and rosette shape (Fig. 8.4a, 8.4b). Increased elongation of petioles at low light (Fig. 8.3b, 8.3d and 8.3b) can be interpreted as shade avoidance reaction (Franklin 2008). The results indicate the importance of exactly defined and controlled environmental conditions and cultivation protocols to avoid variability in experimental results and to increase comparability in

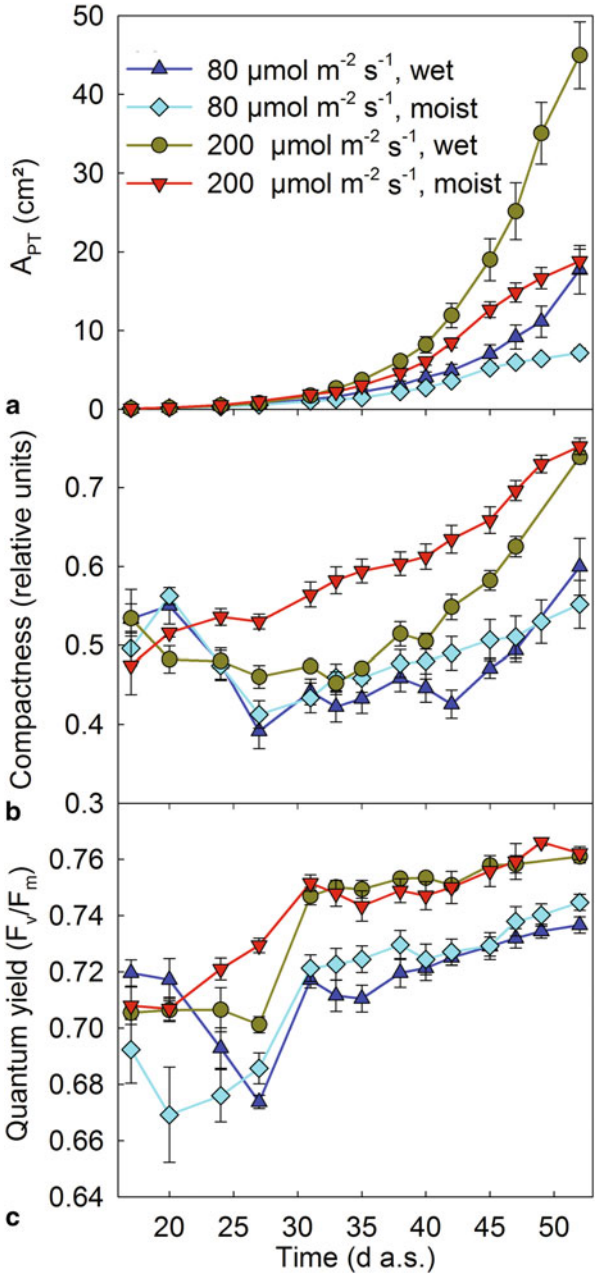

Fig. 8.4 Phenotypic variability of A. thaliana Col-0 grown in two light regimes (80 or 200 µmol m^{-2} s^{-1}) and two soil moisture conditions (moderately moist and wet, n = 8 plants per population, experiment 1): **a** projected leaf area (A_{PT}), **b** rosette compactness, **c** quantum yield of PSII (F_v/F_m); mean values ± SE

successive and multi-site experiments. A recent inter-laboratory comparison experiment resulted in unexpectedly high variability. However, e.g. light intensity varied between 100 and 180 µmol m^{-2} s^{-1} in different labs (Massonnet et al. 2010), which may explain a part of the observed variability. The ratios between A_{PT} and rosette compactness of Col-0 plants at different irrigation and illumination levels assessed

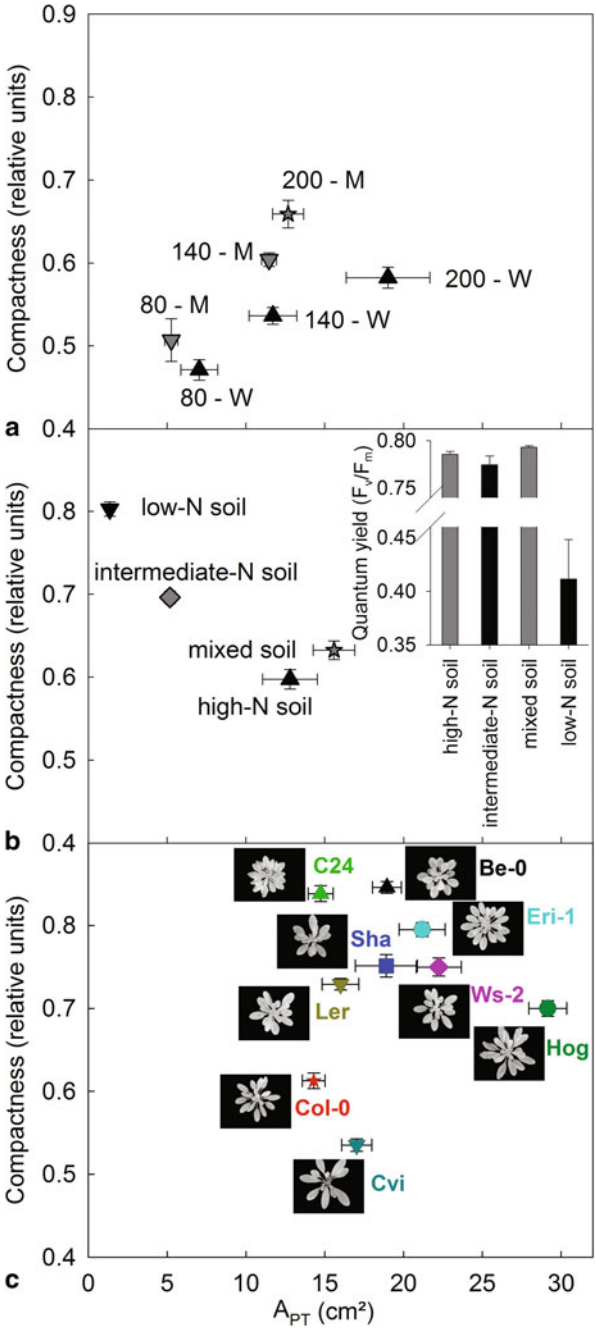

Fig. 8.5 Phenotypic variability of A. thaliana; ratio between projected leaf area (A_{PT}) and rosette compactness of **a** Col-0 grown at different light regimes (PAR values indicated by numbers) and irrigation levels (experiment 1, 45 d a.s.); $n = 8$ plants per population, **b** Col-0 grown in different soil types (experiment 2, 45 d a.s.); insert: quantum yield of PSII (F_v/F_m) of those plants; $n = 16$ plants per population, **c** ecotypes Be-0, C24, Col-0, Cvi, Eri-1, Hog, Ler, Sha, and Ws-2 at the end of vegetative growth (44 d a.s.); $n = 23$ plants per ecotype (experiment 3). Images show representative individuals of each ecotype; mean values ± SE

at 45 d a.s. were influenced independently by soil moisture as well as light intensity (Fig. 8.5a). Generally, an increase in soil moisture changed the ratio in a manner that at similar A_{PT} plants in wet soil were less compact. On the other hand, an increase in

light intensity modulated A_{PT}-to-compactness ratio so that plants with comparable A_{PT} were more compact when grown at higher light intensity.

In experiment 2, *A. thaliana* ecotype Col-0 was grown in five potting substrates differing in nutrient composition and soil structure. At 45 d a.s., plants grown in high-N peat soil and intermediate-N peat-sand-pumice mixed soil had similar A_{PT} ranging between 12.8 and 15.6 cm^2 (Fig. 8.5b), while plants grown in peat soil with either intermediate or low nutrients were significantly smaller (5.2 and 1.4 cm^2, respectively). Although intermediate-N peat soil and mixed soil had similar nutrient concentrations, plants grown in peat reached only a quarter of the size of plants grown in mixed soil. A potential explanation for these results is that not only the total amount of fertilizer is important to sustain growth, but also the soil structure and thus the accessibility of water and nutrients.

Rosette compactness was also affected by the cultivation substrate, e.g. low fertilizer caused not only smaller sizes but also more compact shoot growth (Fig. 8.5b). Apart from plants grown on almost nutrient-free soil that exhibited a strong decrease of F_v/F_m. to 0.4, all plants grown in nutrient richer substrates showed consistent F_v/F_m values of 0.75–0.80 throughout the growth period (Fig. 8.5b, insert). The decrease of low-N plants hints at deficits in PSII functionality at nutrient shortage (Barros and Kuhlbrandt 2009).

At given environmental settings projected leaf area of different *A. thaliana* ecotypes also displayed strong variability (experiment 3, Figs. 8.3f, 8.3c). Differences in A_{PT} developed already early during seedling development (data not shown), which may be due to differences in early seedling vigor or even differences in germination. Later on, similar growth rates in all ecotypes accentuated differences and resulted in considerable diversity in final sizes—the largest ecotype (Hog) reaching a two times larger A_{PT} than the smaller ones (C24 or Col-0; Fig. 8.5c).

Additional strong differences in rosette compactness were found among the ecotypes (Fig. 8.5c). Development of differences in plant size and morphology can be taken as indicators of accumulating impacts throughout the cultivation period determined by ecotype or environment (Fig. 8.5c). Some ecotypes (experiment 3), e.g. Col-0, Ler, and C24 reached similar final A_{PT}, but largely differed in rosette compactness (Fig. 8.5c). Other ecotypes, e.g. Ler, Sha, Ws-2 and Hog, were similar in rosette compactness but differed in A_{PT}.

Intra- and inter-ecotype variability in growth and morphology can be considered as a hallmark of phenotypic plasticity (Reboud et al. 2004). Phenotypic plasticity of a species results from adaptation to natural habitats at the geographic origin and from the ability to cope with environmental stress (Sultan 2000; Koornneef et al. 2004; Pigliucci 2008). In the presented study, we also determined quantum yield of PSII (F_v/F_m), however inter-ecotype differences in F_v/F_m were small throughout the experiment (data not shown).

In summary, phenotypic diversity of *A. thaliana* driven by genetic and environmental factors was clearly shown. Combining phenotypic parameters enables the characterization and quantifying of variability among plant sets in response to genotype and/or environment (Borevitz and Ecker 2004; O'Malley and Ecker 2010). For

the description of a gene function it is necessary to assign the biochemical processes governed by a given gene to physiology and phenotype of the plant (Boyes et al. 2001). Many *A. thaliana* mutants, insertion lines, or activation tagged lines have been investigated to connect phenotypes to genes or genotypes (Bouche and Bouchez 2001; Nakazawa et al. 2003; O'Malley and Ecker 2010). Robust phenotyping methods and exactly designed and recorded protocols (SOPs) are the key to meaningful analyses of gene functions and gene-environment interactions. Moreover, the study shows that it is crucial to precisely control and monitor key environmental factors to which plants are exposed during the experiments. It underlines that—even unwittingly—changed conditions in experimental series with temporal or spatial replications can result in confounding effects.

8.4 Nuclear Magnetic Resonance Imaging (MRI): A Tool for Characterizing and Optimizing the Dynamic Processes of Rhizogenesis and Root Growth of Cuttings

Phenotypic analysis is not only relevant for scientific questions in functional genomics or breeding, but is very valuable in practical plant production. For example vigorous root growth is one phenotypic trait of utmost interest to plant breeders and producers in horticulture. It enables rapid establishment of root systems and, thereby, mechanical support to the plant in a given soil environment, as well as efficient exploration and exploitation of soil resources. Moreover, the potential for rapid development and growth of roots is one essential element of plasticity of the root system to a changing environment. In vegetative multiplication, either for commercial use or for any performance of breeding programs and conservation and restoration programs based on cloning protocols, success notably depends on the phenotypic trait "efficient rooting", i.e., reliable rhizogenesis and subsequent fast growth of the root system. For plant material produced from cuttings the dynamics of root development is in general not directly deducible from shoot development. Shoot and root growth may show different degrees of coupling during the phase of rhizogenesis and initial root growth (Aminah et al. 1997; Costa and Challa 2002; Kovacevic et al. 2009), depending on transpiration conditions and the complex interrelationship of available carbohydrate sources (leaf area) and sinks (roots, buds) (Dick and Dewar 1992). Thus it is difficult to judge in the initial phase of plant propagation whether cuttings will survive or die. Moreover, certain plant species such as *Populus nigra* and other members of the Salicaceae family can exhibit shoot outgrowth from detached leafless shoot parts without any development of roots. As a result, populations of cuttings of such species are particularly difficult to judge regarding the expected survival rates. In breeding, e.g., of ornamental plants, predictions about survival rates of cuttings can only be made based on longer-term experience gained with the respective plant material. Thus for each and every plant line individual long-term collection of information has to be performed—an economically risky situation for nurseries. Selection of breeding lines based on rooting efficiency, as well as optimization of

propagation protocols for plant material with poor rhizogenesis and root growth are still considerably laborious and time-consuming tasks. Since the 1980s numerous studies have been conducted to develop improved rooting protocols (see e.g. the literature cited by Dick and Dewar 1992, and Costa and Challa 2002). However, these studies focused to a large extent on empirical rather than on causal analysis (but see e.g. Aminah et al. 1997; Costa and Challa 2002; Costa et al. 2007) and mostly determined parameters at the end of the experiments with destructive methods, excavating the belowground part of the cutting and quantitatively evaluating its rooting efficiency after washing off the soil. Systematic non-invasive investigations of the causes of poor rooting efficiency including research on the dynamics of rhizogenesis and root system growth were not possible, but can help accelerating and improving the efficiency of practical plant propagation.

In the following, we describe two case studies to use plant phenotyping for developing practical applications. MRI analysis with short measuring times of less than ten minutes per data set was used to characterize roots in soil, to demonstrate the huge potential of MRI to non-invasively elucidate the dynamics of rhizogenesis and growth of newly formed root systems during cultivation of cuttings for vegetative plant propagation. For these studies we selected petunia because of the economic importance for ornamental plant producers to propagate this species as (cost-) efficiently as possible, and because of the fact that homogeneity and reproducibility of rooting efficiency is decisive in this scenario. In addition, poplar was selected because of the above-mentioned difficulty to predict survival rates and rooting efficiency of cuttings based on shoot development alone.

For the case study on petunia, *c*. 5 cm long leafy apical cuttings with initial fresh weight of *c*. 300 mg were prepared for eight different *Petunia* x *hybrida* cultivars, A–H. The cuttings were individually planted in customary 6-cm diameter pots filled with a 2:1 mixture of sand and natural soil from a field site at Kaldenkirchen, Germany. During a 6-week cultivation period, for three individuals per cultivar shoot development was photographically documented on a daily basis, and MRI measurements were performed on selected dates roughly three, four, five and six weeks after planting to non-invasively check for the root development.

MRI measurements were performed at the NMR facility of IBG-2: Plant Sciences, Forschungszentrum Jülich, Germany, using a 4.7 T Varian VNMRS vertical wide-bore MRI system (Varian Inc., Oxford, UK). We used a so-called spin echo experiment, here with an echo time of 6 ms and a repetition time of 1.5 s. Selection of a field of view (FOV) of $6 \times 6\,cm^2$ and a matrix of 128×128 pixels resulted in a total measuring time per data set of 3.2 min and an image resolution of 470 μm. From the image data sets 2D projections over the entire imaged volume were generated after appropriate suppression of the water signals originating from the soil.

During the 6-week observation period for cultivars A, D, G and two out of three individuals of cv. B shoot growth was clearly visible whereas for others, such as C and H, it was hard to decide whether growth took place or not without employing additional technical approaches such as camera-assisted dynamic growth analysis (compare 1.3). Individuals of cultivars E and F occasionally showed yellowing and shedding of leaves towards the end of the observation period. Figure 8.6 gives the root

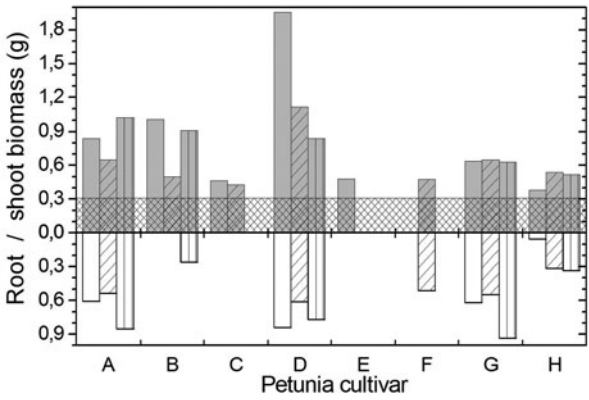

Fig. 8.6 Biomass, given as fresh weight, of roots (*white columns*) and shoots (*gray columns*) of cuttings of eight petunia cultivars A–H after 6-week cultivation as conventionally determined after harvest. The cross-hatched area marks the average initial biomass of the cuttings at the time of planting. Only data for cuttings without black rot are shown

and shoot biomasses (fresh weight) as determined by conventional harvest after 41-d cultivation. The cross-hatched area in the figure marks the average initial biomass of the cuttings at the time of planting, to facilitate judgment on the amount of shoot biomass newly formed during cultivation. Optical inspection of the below-ground part of all still green cuttings revealed black rot on individuals of cultivars C, E and F, which were discarded from the evaluation. Clearly, the investigated cultivars can be grouped into superior performers with regard to rooting efficiency under the given cultivation conditions, namely A, D and G, and inferior performers B, C, E and H. For the two cultivars C and E none of the cuttings managed to develop roots during the observation period with the given cultivation protocol. For B and F only one individual out of three underwent rhizogenesis.

The reasons were, however, apparently different: Whereas F revealed high susceptibility for black rot infestation all cuttings of B remained healthy, suggesting that their rooting was not sufficiently stimulated by the selected protocol. The highest amount of shoot biomass was newly produced by D and individuals of A and B. As a tendency, higher investment into roots compared to shoots was found for cultivars F, G, H and A, whereas for individuals of D and B less investment into roots compared to shoots had obviously taken place.

Non-invasive investigation of the below-ground part of the cuttings with MRI during the 6-week cultivation period added information on the dynamics of rhizogenesis and root growth for the different cuttings. Figure 8.7 shows exemplary MRI data sets for representative cuttings of cultivars A, B and C 26, 34 and 41 days after planting. The selected MRI protocol allows for the distinction of newly formed adventitious roots from the cuttings and also from the soil. The figure reveals that cutting A showed fastest and most vigorous root development and growth. Roots had emerged after 26 days and almost entirely had reached out into the lower half of the pot by the end of the observation period. Compared to cutting A, rooting of cutting B was considerably delayed: Inspection 26 days after planting revealed no roots, but one week later roots were detectable at a similar amount compared to cutting A at time point 26 d (compare Fig. 8.7, B″ and A′). Further observation of cutting B revealed

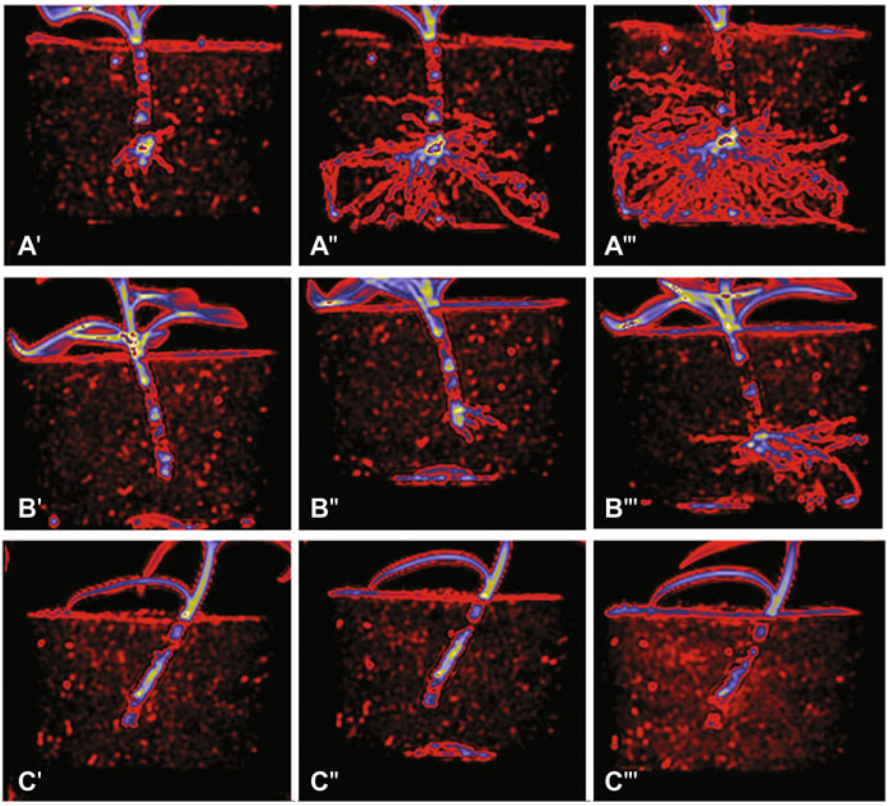

Fig. 8.7 Dynamics of rhizogenesis and progressive root development of individual cuttings of three different petunia cultivars (A, B, C) as revealed by MRI. Measurements were taken 26 d (A′, B′, C′), 34 d (A″, B″, C″) and 41 d after planting (A‴, B‴, C‴). Images represent 2D projections of the signals acquired for the entire volume of the specimen. *Black*, no signal; *red*, low signal intensity; *blue*, medium signal intensity; *yellow*, high signal intensity

less root spreading per day compared to cutting A (compare Fig. 8.7, B″ and A′). This suggests that not only rhizogenesis but also root growth was substantially slower in cultivar B compared to cultivar A—calling for an improved cultivation protocol for this cultivar. Possible reasons for this observation could be a slower metabolism or a lower photosynthetic efficiency in B compared to A, or a different partitioning of photoassimilates into roots and shoots for both cultivars. The latter aspect could be investigated e.g. by a combination of gas exchange, MRI and tracer technologies using short-lived ^{11}C and positron emission tomography, as demonstrated by Jahnke et al. (2009).

For the cutting of cultivar C, no root formation was detectable throughout the entire 41-d cultivation period (Fig. 8.7, C‴), suggesting that the cultivation protocol was insufficient also for this petunia cultivar.

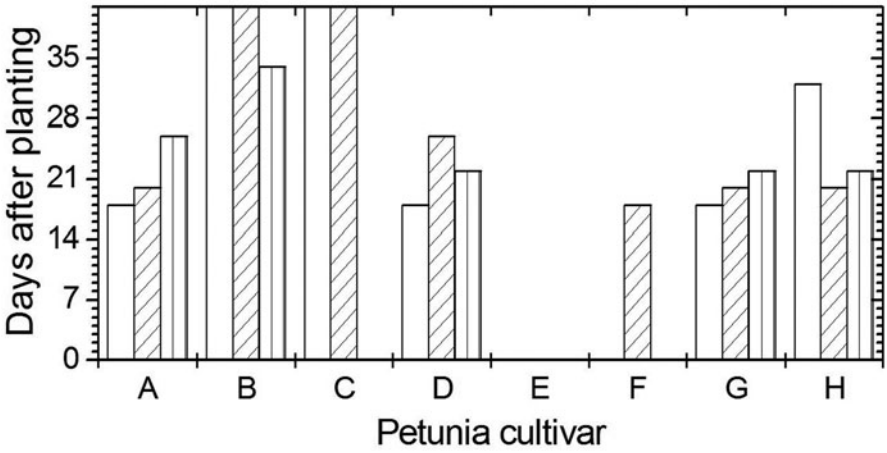

Fig. 8.8 Representation of the dates when roots were first observed with MRI for the individuals of the eight investigated petunia cultivars, A-H. Y > 41 d: no root formation during study. Only data for cuttings without black rot are shown

Cutting B exhibited a substantial increase in MRI signal intensity at its basal end after rhizogenesis had occurred (Fig. 8.7, B″) compared to the situation before rhizogenesis (Fig. 8.7, B′). Also cutting A showed particularly intensive signals at its basal end along with vigorous root growth. This is most likely due to a substantial local increase in new biomass development upon meristem activity for adventitious root formation. No such signal increase is observed for the basal end of cutting C (Fig. 8.7, C′–C‴). On the contrary, a decrease in MRI signal was observed at this spot at day 41 compared to day 34, obviously due to rotting as revealed by destructive inspection. Evaluation of the data sets for all petunia plants measured confirmed that rhizogenesis was always associated with a local high MRI signal at the base of the cutting (see also Fig. 8.9, H1). This feature could even clearly be identified when the overall image quality was comparably poor and roots could hardly be distinguished from soil water, e.g., in case of excess water (data not shown). Thus this MRI analysis method may help to gain high-accuracy and specific datasets on the onset of root formation.

Figure 8.8 summarizes the dates when roots were first observed by MRI for the investigated petunia specimens. It has to be noted that due to technical reasons, in each of the measurement weeks differences of up to four days could occur between the measurements of the different specimens. Cultivars A, D, G and H showed rooting mostly within two to three weeks. Interestingly, the surviving specimen of F also performed fast with roots observable already at day 18, unlike the only rooted specimen of the slow performer cultivar B with roots first detected at day 34 (Fig. 8.7, B″). Homogeneity of root setting, which is an important parameter for commercial plant production, was highest for cultivar G, while individuals of cultivar H showed a roughly 2-week difference of rooting dates.

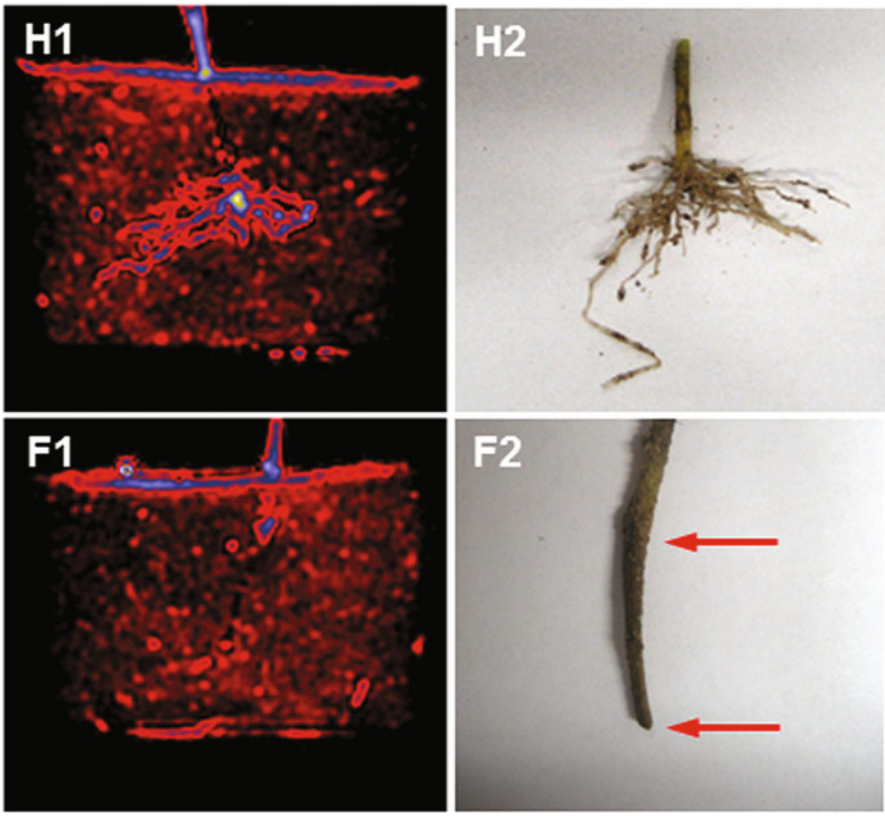

Fig. 8.9 Comparison of root morphologies of individuals from petunia cultivars H and F as revealed by MRI (H1, F1) and photography after excavation (H2, F2) 41 days after planting. The MRI images represent 2D projections of the signals acquired for the entire volume of the specimen. *Black*, no signal; *red*, low signal intensity; *blue*, medium signal intensity; *yellow*, high signal intensity. The *arrows* mark the area of the cutting displaying symptoms of stem black rot

All judgments deduced from MRI whether rooting had taken place or not were confirmed by the results from excavation. Good agreement was also found between the root architecture and morphologies displayed by MRI and the results for the excavated root systems (Fig. 8.9, H1, H2). All cuttings whose basal ends had shown a loss of signal intensity and eventually became indistinguishable from the surrounding soil proved after excavation to be heavily infected by stem black rot (Fig. 8.9, F1, F2).

The good representation of the root morphologies by the MRI 2D projections suggested that calculation of the time courses of root biomass formation for the different petunia cultivars can be achieved on basis of the MRI data. In principle root biomass can be deduced directly from MRI images by multiplying the signal intensity with the pixel volume after calibration against pure water, and by taking into account the usual water content of petunia roots of *c*. 93 % as determined in this study. This was done for single cuttings of the six cultivars which exhibited rooting

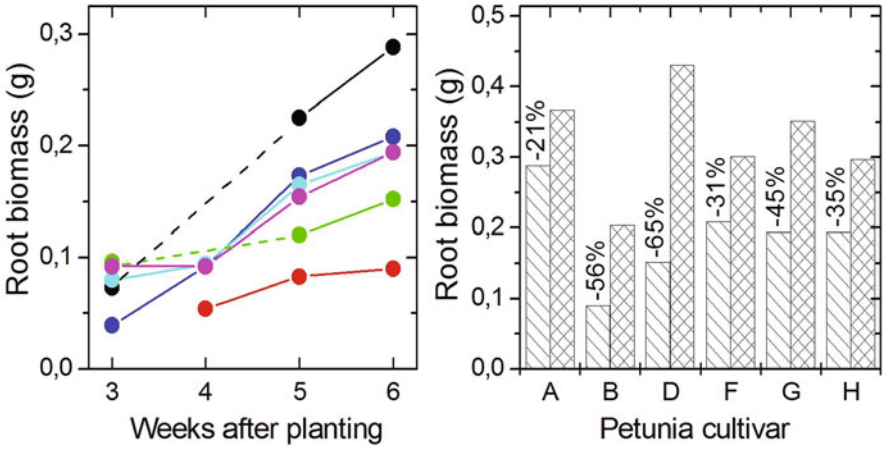

Fig. 8.10 Left: Time course of root biomass development (left) as calculated from MRI 2D projection for individual cuttings from cultivars A (*dark blue dot*), B (*red dot*), D (*lime green dot*), F (*azure blue dot*), G (*aqua dot*) and H (*pink dot*). The *dashed lines* represent extrapolations since single images exhibited too poor quality for quantitative evaluation. Right: Comparison of root biomass for the same samples as determined by MRI (*hatched columns*) and conventionally (*cross-hatched columns*) 41 days after planting. The numbers give the percentage deviation of the MRI results from the real biomass

(Fig. 8.10, left). All time courses show a reasonable increase of root biomass from an initial, comparably low value to the final value during the 41-day observation period. Steepest slopes for root biomass formation (10 mg d^{-1} and 8 mg d^{-1}) were determined for the root systems of the cuttings from cultivars A and F, respectively. Cuttings from B and D exhibited with 2 and 3 mg d^{-1}, respectively, substantially more shallow slopes. Interestingly, the growth of the cuttings from cultivars G and H appeared somewhat slower at the initial compared to later stages, whereas the root system of the cutting from cultivar F showed a more or less constant growth speed throughout the entire observation period. Comparison with the data for the excavated cuttings, however, revealed that the MRI-derived values underestimated the real root biomass at the endpoint of the study by 21–65 % (Fig. 8.10, right).

This pronounced deviation is most likely due to highly discriminating setting of threshold values for subtraction of background water signal: Due to selection of a comparatively high threshold, smaller roots with diameters that are smaller than the edge length of a pixel volume (voxel) are rejected for analysis, thereby causing a considerable reduction of the detected root mass. This effect would get bigger at larger voxel sizes or smaller root diameters.

The reported data suggest that useful MRI images can be obtained for soil-cultivated petunia cuttings within a relatively short measuring time of only 3 minutes and thus can provide a valuable tool for categorizing rooting efficiency of cultivars and for guided improvement of propagation protocols, but also in other phenotyping experiments. The accuracy of the method can be further enhanced by opting for additional averages, at the cost of additional measurement time, and by reducing the

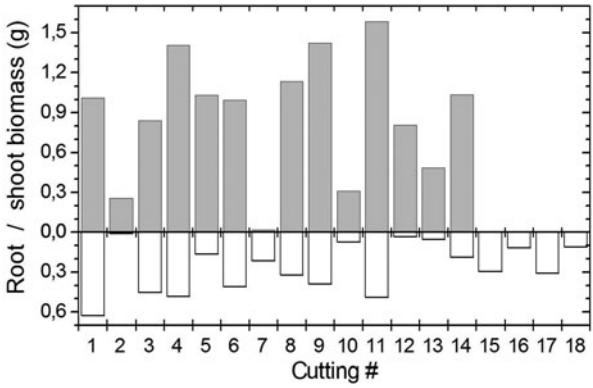

Fig. 8.11 Biomass of newly formed roots (*white columns*) and shoots (*gray columns*) of 18 rooted cuttings of cottonwood after 3-week cultivation, given as fresh weight conventionally determined after harvest

soil water content, to facilitate proper setting of the lower threshold for quantitative evaluation.

The second MRI case study comprised 54 6-cm-long leafless cuttings of Eastern cottonwood (*Populus deltoides*) taken from semi-hardwood shoot parts of 26 greenhouse-grown 6-month-old plants. The same type of pots and sand/soil mixture were used as for the petunias, for three-week cultivation. Many of the cuttings showed very fast outgrowth of shoots from buds which had reached heights of up to 2 cm already one week after planting. By the end of the three-week observation period, a high percentage of the shoot-bearing cuttings had formed up to three outgrowths with maximum shoot lengths of 8.5 cm. In total, 41 out of the 54 cuttings (76 %) developed shoots, but three of them died and experienced rotting before the end of the experiment. Additional six cuttings showed symptoms of stem black rot without forming shoots. Five cuttings (9 %) had developed neither shoots nor roots. Only 29 of the shoot-exhibiting cuttings (54 %) had additionally undergone rhizogenesis and root growth. Four individuals had formed roots without forming shoots, thus eventually increasing the percentage of rooted cuttings to 61 % in this study. These results match very well with results from a parallel study on 103 *P. deltoides* cuttings cultivated in commercial propagation substrate under comparable environmental conditions, yielding 71 % and 59 % shoot and root outgrowth, respectively.

Root and shoot biomasses and the respective root/shoot ratios of the cuttings in our MRI study substantially varied between the individuals as shown in Fig. 8.11 for 14 out of the 29 cuttings that exhibited root as well as shoot outgrowth. The root biomass formed by the cuttings which had not developed shoots also considerably varied and occasionally exceeded the values determined for the cuttings with both root and shoot formation (Fig. 8.11).

Consecutive MRI measurements on 24 out of the 54 cuttings two and three weeks after planting added further information regarding the dynamics of root formation and growth of the different cuttings under investigation. The spin echo sequence used featured the same values for echo and repetition times as for the petunias. Selection of FOV $= 7.5 \times 7.5\,\text{cm}^2$ and a 256×256 matrix resulted in a measuring time per data set of 6.5 min and an image resolution of 290 μm in this study. As shown

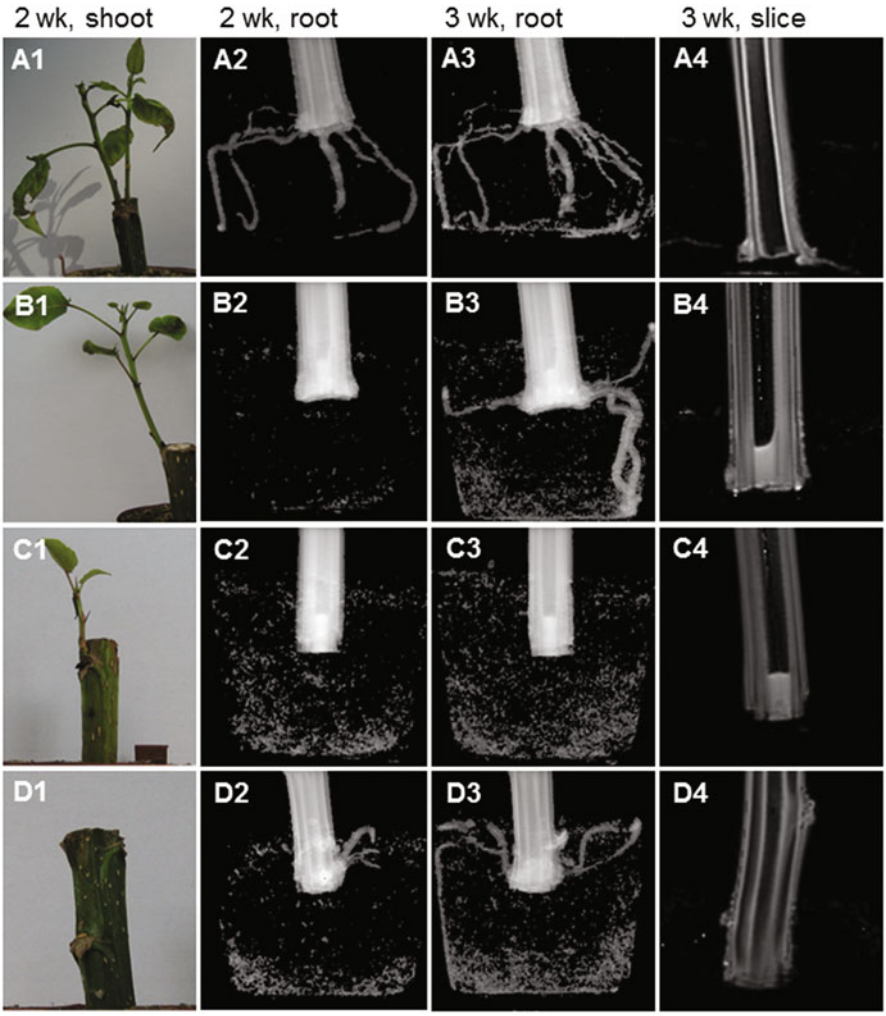

Fig. 8.12 Four examples of shoot development as documented by eye, and root development as documented by 2D MRI projection images, for cuttings of *Populus deltoides*. Two weeks after planting three out of the four cuttings exhibited shoot outgrowth (A1, B1, C1). Roots, however, had developed at the same time only for cuttings A (A2) and D (D2). A rescan of all specimens after 3-week cultivation revealed that cutting B obviously experienced delayed root outgrowth compared to cuttings A and D (see B3) whereas yet no rooting had occurred for cutting C (C3). Images A4, B4, C4 and D4 represent 5-mm-thick sagittal virtual slices of the respective cuttings after 3-week cultivation

in Fig. 8.12 newly formed adventitious roots could clearly be distinguished from the cuttings and also from the soil water by the selected method. 17 out of the 24 cuttings showed rooting. MRI revealed a very good recognition of the four types of outgrowth, namely shoot and root (Fig. 8.12a, 8.12b), shoot but no root (Fig. 8.12c),

no shoot but root (Fig. 8.12d), and no shoot and no root (data not shown). As for the petunias, all results from excavation confirmed the results from MRI about rooting events of the poplar cuttings.

MRI also revealed differences in the dynamics of root formation as shown for the petunias. For eleven out of the 17 rooted cuttings (65 %) rooting had already occurred earlier than two weeks after planting (compare Fig. 8.12, A2 and D2). At the time point two weeks after planting the size of the developed root systems varied considerably (Fig. 8.12, A2 and D2). The well-known phenomenon of substantial shoot outgrowth without simultaneous rooting could frequently be documented in this MRI study, as exemplified for cuttings B and C in Fig. 8.12.

More than two weeks after planting, however, many of the respective cuttings eventually showed rhizogenesis. As for the petunias, many poplar cuttings showed particularly high signal intensities at their basal ends (Fig. 8.12, B2/3, C2/3, D2/3). Sagittal virtual slices obtained with MRI of the respective specimens after 3-week cultivation showed that a signal-rich substance had obviously accumulated predominantly in the basal pith region of these specimens (Fig. 8.12, suffices 4). This feature was detected with MRI in 14 cuttings in total, irrespective of being rooted or rootless (Fig. 8.12, B4, C4, D4). On the other hand, it could be absent in cuttings showing particularly vigorous rooting (Fig. 8.12, A4), suggesting that it was not an essential prerequisite for rhizogenesis and/or root growth. Thus, unlike for petunia, particularly high basal MRI signals could not be taken as clear-cut indication for rhizogenesis in the case of the poplar cuttings. Meristems for adventitious root growth, however, could be detected by MRI as smooth, rounded shapes along the otherwise sharp contours of the cuttings (Fig. 8.12, A4, B4, D4). Evaluation of all MRI datasets suggested that cuttings of *P. deltoides* reveal this change of shape obviously substantially earlier compared to the time point when root outgrowth is detectable (Fig. 8.12, B2). By contrast, a cutting which has experienced no rhizogenesis persistently exhibits sharp contours (Fig. 8.12, C3). Thus, the feature of "shape smoothing" may be a valuable trait for optimization of propagation protocols for poplar.

The two presented case studies for petunia and poplar cuttings, though being preliminary due to low sample numbers, show that non-invasive MRI studies could be a valuable tool for the development of phenotyping protocols to optimize vegetative propagation protocols and, thus, the rooting efficiency of cuttings for commercial use, breeding and conservation programs. We have shown that the use of measuring protocols of 3–7 min yielded sufficient image resolution to detect newly formed roots, to elucidate the initial steps of the rooting process of the cuttings and to document the subsequent development of the root systems. In the case of petunia, the study allowed a preliminary categorization of eight cultivars with respect to their rooting efficiency and sensitivity to propagation protocols, based on detection of the time points of root outgrowth and the occurrence of particularly high MRI signal intensities at the base of the cutting. For poplar, indications for the determination of the initial step of root formation based on "shape smoothing" of the basal end of the cutting could be dissected. An explanation for the observed heterogeneity of root and shoot formation could, however, not yet be elaborated.

When using the presented relatively fast measuring protocols the amount of specimens that can be measured on a daily basis with MRI is not so much restricted by the measurement time itself but by the manual positioning of the specimens within the MRI magnet. Recently, we successfully tested a setup with a robot for automated positioning of the specimens in the magnet at the NMR facility of IBG-2: Plant Sciences, Forschungszentrum Jülich, Germany, which in combination with the presented protocols will allow for medium-throughput approaches handling up to *c*. 100 of such small specimens per day. Also, the 2D signal projection provides a time-saving, straightforward approach for data reconstruction and evaluation. More effort, however, has to be put into the development of suitable protocols for proper calculation of root biomass from the 2D signal projections, to allow for additional non-invasive investigations of the dynamic development of root/shoot ratios during the process of rooting. These kinds of measurements can likewise be used to elucidate above- and below-ground dynamics of growth in the presence of biotic and abiotic stresses including nutrient deficiency and drought, and there are many more applications to be addressed with the presented protocols.

8.5 Conclusions

Non-invasive methodologies for the accurate description of plant phenotypes and their dynamic interaction with main environmental factors are invaluable to address the genome to phenome bottleneck (Furbank and Tester 2011) in scientific as well as practical applications. In particular, novel imaging technologies are extensively evaluated by various research groups. Notably, 2D visible and fluorescence imaging are used today for genotype screening. MRI offers unique opportunities for structural-functional analyses especially for studies on the dynamics of root growth and transport in roots. At the field scale, remote sensing of canopy function is constantly increasing its arsenal of sensors and measured parameters and imaging spectroscopy opens a wide range of indices that are related to aboveground traits. We stressed that several technological challenges remain to be addressed to further increase precision, accuracy, robustness and—in some cases—measuring speed and throughput of these methods. In addition, beyond 'taking pictures', correct interpretation often requires in-depth understanding of sensor physics and of the biology of the targeted organs. Interestingly, several applications can be used to phenotype a growing number of genetic resources, individually or in combined approaches.

Acknowledgments The authors would like to thank Silvia Braun (case study 2) and Martina Klein, Sabrina Lauter and Carola Mohl (case study 3) for excellent technical assistance. Experiments in case study 1 were supported by Bundesministerium für Bildung und Forschung (BMBF, Germany) in the CROP.SENSe.net consortium. Francisco Pinto was supported by Deutscher Akademischer Austauchdienst (DAAD, Germany) and the Commission for Scientific and Technological Research (CONICYT, Chile). Development of the MRI protocol for petunia in case study 3 was supported by a grant from Bundesministerium für Ernährung, Landwirtschaft und Verbraucherschutz (BMELV, Germany) via Bundesanstalt für Landwirtschaft und Ernährung (BLE, Germany) in the framework of Programm zur Innovationsförderung.

References

Aminah H, Dick JM, Grace J (1997) Rooting of *Shorea leprosula* stem cuttings decreases with increasing leaf area. Forest Ecol Manag 91:247–254

Armengaud P, Zambaux K, Hills A et al (2009) EZ-rhizo: integrated software for the fast and accurate measurement of root system architecture. Plant J 57:945–956

Arvidsson S, Perez-Rodriguez P, Mueller-Roeber B (2011) A growth phenotyping pipeline for *Arabidopsis thaliana* integrating image analysis and rosette area modeling for robust quantification of genotype effects. New Phytol 191:895–907

Barros T, Kuhlbrandt W (2009) Crystallisation, structure and function of plant light-harvesting complex II. Biochim Biophys Acta 1787:753–772

Barton CVM, North PRJ (2001) Remote sensing of canopy light use efficiency using the photochemical reflectance index—model and sensitivity analysis. Remote Sens Environ 78:264–273

Berger B, Parent B, Tester M (2010) High-throughput shoot imaging to study drought responses. J Exp Bot 61:3519–3528

Blackburn GA (2007) Hyperspectral remote sensing of plant pigments. J Exp Bot 58:855–867

Borevitz JO, Ecker JR (2004) Plant genomics: the third wave. Annu Rev Genom Hum Genet 5:443–477

Bottomley PA, Rogers HH, Foster TH (1986) NMR imaging shows water distribution and transport in plant root systems *in situ*. P Natl Acad Sci U S A 83:87–89

Bottomley PA, Rogers HH, Prior SA (1993) NMR imaging of root water distribution in intact *Vicia faba* L. plants in elevated atmospheric CO_2. Plant Cell Environ 16:335–338

Bouche N, Bouchez D (2001) *Arabidopsis* gene knockout: phenotypes wanted. Curr Opin Plant Biol 4:111–117

Boyes DC, Zayed AM, Ascenzi R et al (2001) Growth stage-based phenotypic analysis of *Arabidopsis*: a model for high throughput functional genomics in plants. Plant Cell 13:1499–1510

Brown DP, Pratum TK, Bledsoe C et al (1991) Noninvasive studies of conifer roots: nuclear magnetic resonance (NMR) imaging of Douglas-fir seedlings. Can J Forest Res 21:1559–1566

Carminati A, Moradi AB, Vetterlein D et al (2010) Dynamics of soil water content in the rhizosphere. Plant Soil 332:163–176

Chen JM, Li X, Nilson T, Strahler A (2000) Recent advances in geometrical optical modelling and its applications. Remote Sens Rev 18:227–262

Christensen S, Goudriaan J (1993) Deriving light interception and biomass from spectral reflectance ratio. Remote Sens Environ 43:87–95

Clark RT, MacCurdy RB, Jung JK et al (2011) Three-dimensional root phenotyping with a novel imaging and software platform. Plant Physiol 156:455–465

Costa JM, Challa H (2002) The effect of the original leaf area on growth of softwood cuttings and planting material of rose. Sci Hortic 95(1–2):111–121

Costa JM, Heuvelink E, Van de Pol PA, Put HMC (2007) Anatomy and morphology of rooting in leafy rose stem cuttings and starch dynamics following severance. Acta Hortic 751:495–502

Danson FM, Steven MD, Malthus TJ, Clark JA (1992) High-spectral resolution data for determining leaf water content. Int J Rem Sens 13(3):461–470

Dick JMcP, Dewar RC (1992) A mechanistic model of carbohydrate dynamics during adventitious root development of leafy cuttings. Ann Bot 70:371–377

Eiden M, Linden S van der, Schween JH et al (2007) Elucidating physiology of plant mediated exchange processes using airborne hyperspectral reflectance measurements an synopsis with eddy covariance data. In: 10th ISPMSRS Conference, March 12–14, 2007, Davos, pp 473–481

Feilhauer H, Asner GP, Martin RE, Schmidtlein S (2010) Brightness-normalized partial least squares regression for hyperspectral data. J Quant Spectrosc Radiat Transf 111:1947–1957

Franklin KA (2008) Shade avoidance. New Phytol 179:930–944

Furbank RT, Tester M (2011) Phenomics—technologies to relieve the phenotyping bottleneck. Trends Plant Sci 16:635–644

Gamon JA, Field CB, Bilger W et al (1990) Remote sensing of the xanthophyll cycle and chlorophyll fluorescence in sunflower leaves and canopies. Oecologia 85:1–7
Gamon JA, Peuelas J, Field CB (1992) A narrow-waveband spectral index that tracks diurnal changes in photosynthetic efficiency. Remote Sens Environ 41(1):35–44
Garbulsky MF, Peuelas J, Gamon J et al (2011) The photochemical reflectance index (PRI) and the remote sensing of leaf, canopy and ecosystem radiation use efficiencies: a review and meta-analysis. Remote Sens Environ 115(2):281–297
Gitelson AA, Zur Y, Chivkunova OB, Merzlyak MN (2002) Assessing carotenoid content in plant leaves with reflectance spectroscopy. Photochem Photobiol 75(3):272–281
Gitelson AA, Chivkunova OB, Merzlyak MN (2009) Nondestructive estimation of anthocyanins and chlorophylls in anthocyanic leaves. Am J Bot 96(10):1861–1868
Goel NS (1988) Models of vegetation canopy reflectance and their use in estimation of biophysical parameters from reflectance data. Remote Sens Rev 4:1–122
Goel NS (1989) Inversion of canopy reflectance models for estimation of biophysical parameters from reflectance data. In: Asrar G (ed) Theory and applications of optical remote sensing. Wiley, New York, pp 205–251
Golzarian MR, Frick RA, Rajendran K et al (2011) Accurate inference of shoot biomass from high-throughput images of cereal plants. Plant Methods 7:2
Granier C, Aguirrezabal L, Chenu K et al (2006) PHENOPSIS, an automated platform for reproducible phenotyping of plant responses to soil water deficit in *Arabidopsis thaliana* permitted the identification of an accession with low sensitivity to soil water deficit. New Phytol 169:623–635
Gregory PJ, Hutchison DJ, Read DB et al (2003) Non-invasive imaging of roots with high resolution X-ray micro-tomography. Plant Soil 255:351–359
Guo JM, Trotter CM (2004) Estimating photosynthetic light-use efficiency using the photochemical reflectance index: variations among species. Funct Plant Biol 31:255–265
Haboudane D, Miller JR, Pattey E et al (2004) Hyperspectral vegetation indices and novel algorithms for predicting green LAI of crop canopies: modeling and validation in the context of precision agriculture. Remote Sens Environ 90:337–352
Hansen PM, Schjoerring JK (2003) Reflectance measurement of canopy biomass and nitrogen status in wheat crops using normalized difference vegetation indices and partial least squares regression. Remote Sens Environ 86:542–553
Hargreaves CE, Gregory PJ, Bengough AG (2009) Measuring root traits in barley (*Hordeum vulgare* ssp. *vulgare* and ssp. *spontaneum*) seedlings using gel chambers, soil sacs and X-ray microtomography. Plant Soil 316:285–297
Heeraman DA, Hopmans JW, Clausnitzer V (1997) Three dimensional imaging of plant roots in situ with X-ray computed tomography. Plant Soil 189:167–179
Hillnhütter C, Sikora RA, Oerke E-C, Dusschoten D van (2012) Nuclear magnetic resonance: a tool for imaging below-ground damage caused by *Heterodera schachtii* and *Rhizoctonia solani* on sugar beet. J Exp Bot 63(1):319–327
Hostert P, Diermayer E, Damm A, Schiefer S (2005) Spectral unmixing based on image and reference endmembers for urban change analysis. In: 24th Symposium of the European-Association-of-Remote-Sensing-Laboratories (EARSeL), May 25-27, 2004, Dubrovnik. New strategies for European remote sensing, pp 645–652
Hurlbert SH (1984) Pseudoreplication and the design of ecological field experiments. Ecol Monogr 54:187–211
Iyer-Pascuzzi AS, Symonova O, Mileyko Y et al (2010) Imaging and analysis platform for automated phenotyping and trait ranking of plant root systems. Plant Physiol 152:1148–1157
Jackson RD, Huete AR (1991) Interpreting vegetation indexes. Prev Vet Med 11:185–200
Jahnke S, Menzel MI, van Dusschoten D et al (2009) Combined MRI-PET dissects dynamic changes in plant structures and functions. Plant J 59(4):634–644
Jansen M, Gilmer F, Biskup B et al (2009) Simultaneous phenotyping of leaf growth and chlorophyll fluorescence via GROWSCREEN FLUORO allows detection of stress tolerance in *Arabidopsis thaliana* and other rosette plants. Funct Plant Biol 36:902–914

Knipling EB (1970) Physical and physiological basis for the reflectance of visible and near-infrared radiation from vegetation. Remote Sens Environ 1(3):155–159

Kolber Z, Klimov D, Ananyev G et al (2005) Measuring photosynthetic parameters at a distance: laser induced fluorescence transient (LIFT) method for remote measurements of PSII in terrestrial vegetation. Photosynth Res 84:121–129

Koornneef M, Alonso-Blanco C, Vreugdenhil D (2004) Naturally occurring genetic variation in *Arabidopsis thaliana*. Annu Rev Plant Biol 55:141–172

Kovacevic B, Roncevic S, Miladinovic D et al (2009) Early shoot and root growth dynamics as indicators for the survival of black poplar cuttings. New Forest 38:177–185

Kümmerlen B, Dauwe S, Schmundt D, Schurr U (1999) Thermography to measure water relations of plant leaves Volume 3, systems and applications. In: Jähne B, Haussecker H, Geissler P (eds). Handbook of computer vision and applications. Academic, pp 763–781

Malenovský Z, Mishra KB, Zemek F et al (2009) Scientific and technical challenges in remote sensing of plant canopy reflectance and fluorescence. J Exp Bot 60:2987–3004

Massonnet C, Vile D, Fabre J et al (2010) Probing the reproducibility of leaf growth and molecular phenotypes: a comparison of three *Arabidopsis* accessions cultivated in ten laboratories. Plant Physiol 152:2142–2157

Meininger M, Jakob PM, von Kienlin M et al (1997) Radial spectroscopic imaging. J Magn Reson 125(2):325–331

Menzel MI, Oros-Peusquens A-M, Pohlmeier A et al (2007) Comparing 1H-NMR imaging and relaxation mapping of German white asparagus from five different cultivation sites. J Plant Nutr Soil Sci 170:24–38

Merzlyak MN, Gitelson AA, Pogosyan SI et al (1997) Reflectance spectra of plant leaves and fruits during their development, senescence and under stress. Russ J Plant Physiol 44:614–622

Merzlyak MN, Gitelson AA, Chivkunova OB, Rakitin VYU (1999) Non-destructive optical detection of pigment changes during leaf senescence and fruit ripening. Physiol Plantarum 106(1):135–141

Mittler R, Blumwald E (2010) Genetic engineering for modern agriculture: challenges and perspectives. Annu Rev Plant Biol 61:443–462

Moradi AB, Carminati A, Vetterlein D et al (2011) Three-dimensional visualization and quantification of water content in the rhizosphere. New Phytol 192:653–663

Moya I, Camenen L, Evain S et al (2004) A new instrument for passive remote sensing 1. Measurements of sunlight-induced chlorophyll fluorescence. Remote Sens Environ 91:186–197

Munns R, James RA, Sirault XRR et al (2010) New phenotyping methods for screening wheat and barley for beneficial responses to water deficit. J Exp Bot 61:3499–3507

Myneni RB, Ross J, Asrar G (1989) A review on the theory of photon transport in leaf canopies. Agr Forest Meteorol 45:1–153

Nagel KA, Kastenholz B, Jahnke S et al (2009) Temperature responses of roots: impact on growth, root system architecture and implications for phenotyping. Funct Plant Biol 36:947–959

Nagel KA, Putz A, Gilmer et al (2012) GROWSCREEN-Rhizo is a novel phenotyping robot enabling simultaneous measurements of root and shoot growth for plants grown in soil-filled rhizotrons. Funct Plant Biol. doi:10.1071/FP12023 39(11):891–904

Nakazawa M, Ichikawa T, Ishikawa A et al (2003) Activation tagging, a novel tool to dissect the functions of a gene family. Plant J 34:741–750

O'Malley RC, Ecker JR (2010) Linking genotype to phenotype using the *Arabidopsis* unimutant collection. Plant J 61:928–940

Osmond CB, Daley PF, Badger MR, Lüttge U (1998) Chlorophyll fluorescence quenching during photosynthetic induction in leaves of *Abutilon striatum* Dicks. infected with Abutilon mosaic virus, observed with a field-portable imaging system. Bot Acta 111:390–397

Passioura J (2010) Scaling up: the essence of effective agricultural research. Funct Plant Biol 37:585–591

Pierret A, Kirby M, Moran C (2003) Simultaneous X-ray imaging of plant root growth and water uptake in thin-slab systems. Plant Soil 255:361–373

Pigliucci M (2008) Ecology and evolutionary biology of *Arabidopsis*. *Arabidopsis* Book 1:e0003. doi:10.1199/tab.0003

Purdue University (2011) 101 ways to grow *Arabidopsis*. http://www.hort.purdue.edu/hort/facilities/greenhouse/101exp.shtml. Accessed 1 Dec 2011

Rascher U, Nichol CJ, Small C, Hendricks L (2007) Monitoring spatio-temporal dynamics of photosynthesis with a portable hyperspectral imaging system. Photogramm Eng Rem Sens 73:45–56

Rascher U, Agati G, Alonso L et al (2009) CEFLES2: the remote sensing component to quantify photosynthetic efficiency from the leaf to the region by measuring sun-induced fluorescence in the oxygen absorption bands. Biogeosciences 6:1181–1198

Rascher U, Damm A, van der Linden S et al (2010) Sensing of photosynthetic activity of crops. In: EC et al O (eds) Precision crop protection—the challenge and use of heterogeneity. Springer Science + Business Media BV, pp 87–99. doi:10.1007/978-90-481-9277-9_6

Rascher U, Blossfeld S, Fiorani F et al (2011) Non-invasive approaches for phenotyping of enhanced performance traits in bean. Funct Plant Biol 38:968–983

Reboud X, Le Corre V, Scarcelli N et al (2004) Natural variation among accessions of *Arabidopsis thaliana*: beyond the flowering date, what morphological traits are relevant to study adaptation? In: Cronk QCB, Whitton J, Ree RH, Taylor IEP (eds) Plant adaptation: molecular genetics and ecology. Natl Research Council Canada, Ottawa, pp 135–142

Richards RA (2000) Selectable traits to increase crop photosynthesis and yield of grain crops. J Exp Bot 51:447–458

Rogers HH, Bottomley PA (1987) *In situ* magnetic resonance imaging of roots: influence of soil type, ferromagnetic particle content, and soil water. Agron J 79:957–965

Rokitta M, Peuke AD, Zimmermann U, Haase A (1999) Dynamic studies of phloem and xylem flow in fully differentiated plants by fast nuclear-magnetic-resonance microimaging. Protoplasma 209:126–131

Rollin EM, Milton EJ (1998) Processing of high spectral resolution reflectance data for the retrieval of canopy water content information. Remote Sens Environ 65(1):86–92

Römer C, Wahabzada M, Ballvora A et al (2012) Early drought stress detection in cereals: simplex volume maximization for hyperspectral image analysis. Funct Plant Biol 39:878–890

Schilling M, Pfeifer AC, Bohl S, Klingmuller U (2008) Standardizing experimental protocols. Curr Opin Biotech 19:354–359

Simpson AJ, McNally DJ, Simpson MJ (2011) NMR spectroscopy in environmental research: from molecular interactions to global processes. Prog Nucl Magn Reson Spectrosc 58:97–175

Skirycz A, Vandenbroucke K, Clauw P et al (2011) Survival and growth of *Arabidopsis* plants given limited water are not equal. Nat Biotechnol 29:212–214

Stylinski CS, Gamon JG, Oechel WO (2002) Seasonal patterns of reflectance indices, carotenoid pigments and photosynthesis of evergreen chaparral species. Oecologia 131(3):366–374

Sultan SE (2000) Phenotypic plasticity for plant development, function and life history. Trends Plant Sci 5:537–542

Turner DP, Cohen WB, Kennedy RE et al (1999) Relationships between leaf area index and landsat TM spectral vegetation indices across three temperate zone sites. Remote Sens Environ 70:52–68

Ustin S, Gamon JA (2010) Remote sensing of plant functional types. New Phytol 186:795–816

As H van (2007) Intact plant MRI for the study of cell water relations, membrane permeability, cell-to-cell and long distance water transport. J Exp Bot 58:743–756

As H van, Scheenen T, Vergeldt FJ (2009) MRI of intact plants. Photosynth Res 102:213–222

Verrelst J, Schaepman ME, Koetz B, Kneubühler M (2008) Angular sensitivity analysis of vegetation indices derived from CHRIS/PROBA data. Remote Sens Environ 112:2341–2353

Walter A, Schurr U (2005) Dynamics of leaf and root growth: endogenous control versus environmental impact. Ann Bot 95:891–900

Walter A, Rascher U, Osmond CB (2004) Transition in photosynthetic parameters of midvein and interveinal regions of leaves and their importance during leaf growth and development. Plant Biol 6:184–191

Walter A, Scharr H, Gilmer F et al (2007) Dynamics of seedling growth acclimation towards altered light conditions can be quantified via GROWSCREEN: a setup and procedure designed for rapid optical phenotyping of different plant species. New Phytol 174:447–455

Walter A, Silk WK, Schurr U (2009) Environmental effects on spatial and temporal patterns of leaf and root growth. Annu Rev Plant Biol 60:279–304

Weigel D, Glazebrook J (2002) *Arabidopsis*: a laboratory manual. Cold Spring Harbor Laboratory Press, Cold Spring Harbor

Zadoks JC, Chang TT, Konzak CF (1974) A decimal code for the growth stages of cereals. Weed Res 14:415–421 and Eucarpia Bull 7:49–52

Zhu J, Ingram PA, Benfey PN, Elich T (2011) From lab to field, new approaches to phenotyping root system architecture. Curr Opin Plant Biol 14:310–317